International Conference on Space Optics—ICSO 2006

Noordwijk, Netherlands

27–30 June 2006

Edited by Errico Armandillo, Josiane Costeraste, and Nikos Karafolas

Large aperture and wide field of view space telescope for the detection of ultra high energy cosmic rays and neutrinos

Piero Mazzinghi, Vojko Bratina, Lisa Gambicorti,
Francesca Simonetti, et al.

LARGE APERTURE AND WIDE FIELD OF VIEW SPACE TELESCOPE FOR THE DETECTION OF ULTRA HIGH ENERGY COSMIC RAYS AND NEUTRINOS

Piero Mazzinghi[(1)], Vojko Bratina[(1)], Lisa Gambicorti[(1,2)], Francesca Simonetti[(1)], Alessandro Zuccaro Marchi[(1)]

[(1)]*National Institute of Applied Optics (INOA-CNR), Largo E. Fermi, 6 – 50125 Firenze, Italy*
[(2)]*Dept. of Astronomy and Space Science, Florence University, Largo E. Fermi, 2 – 50125 Firenze, Italy*
Emails: piero.mazzinghi@inoa.it, vojko.bratina@inoa.it, lisa.gambicorti@inoa.it, francesca.simonetti@inoa.it, alessandro.zuccaro@inoa.it

ABSTRACT

New technologies are proposed for large aperture and wide Field of View (FOV) space telescopes dedicated to detection of Ultra High Energy Cosmic Rays and Neutrinos flux, through observation of fluorescence traces in atmosphere and diffused Čerenkov signals.

The presented advanced detection system is a spaceborne LEO telescope, with better performance than ground-based observatories, detecting up to 10^3-10^4 events/year. Different design approaches are implemented, all with very large FOV and focal surface detectors with sufficient segmentation and time resolution to allow precise reconstructions of the arrival direction. In particular, two Schmidt cameras are suggested as an appropriate solution to match most of the optical and technical requirements: large FOV, low f/#, reduction of stray light, optionally flat focal surface, already proven low-cost construction technologies. Finally, a preliminary proposal of a wide-FOV retrofocus catadioptric telescope is explained.

Key words: Schmidt camera, focal surface, cosmic rays, fluorescence shower.

1. INTRODUCTION

Ultra High Energy Cosmic Rays (UHECRs) are generally unknown events that travel throughout the universe. Approaching the atmosphere, they interact mainly with Nitrogen molecules and produce a cascade of secondary particles (Extensive Air Shower, EAS), which give rise to a faint streak of fluorescence light (with three main peaks of 337, 357 and 391 nm) indicating the trajectory of the primary cosmic ray [1] and to Cherenkov light. However, there is still no prediction about when and where these events take place in the atmosphere, so many samples are needed to provide physical insight and justification to existing astronomical theories, and a devoted experiment must continuously observe a large portion of the atmosphere. Today's systems for UHECR detection through induced fluorescence consist of very large arrays of detectors (eg. scintillators, Cherenkov detectors) deployed on the ground over many square kilometres [2] [3], observing a small portion of the sky. However, the flux of UHECRs above 10^{19} eV is low, and the rate of detectable neutrinos is far less. The ground-based observatories have detected so far only a few dozens of events, representing a poor statistic.

Because of unforeseeable origin directions and faint available signal, an EAS observatory would benefit if lifted to space, since it would allow an inspection of a bigger atmospheric target, thus providing a wider statistic. Such a space-borne telescope must be ideated with new instrumentation providing large Field of View (FOV) and aperture in order to increase the probability of detection. Recently proposed optical design solutions [4] for Schmidt-type telescopes demonstrated that a combination of segmented mirrors and refractive surfaces, driven by active optics elements, can overcome this problem, resulting in very big aperture Schmidt telescope (up to 4m in diameter). Building telescopes with higher apertures and mirrors is therefore one of the technology challenges of the future, and it may open the view to many new applications for space astrophysics.

Among the various possible design approaches for the optics, a catadioptric system made with Schmidt corrector is the one which most matches the needed optical and technical requirements for cosmic rays analysis. The description of two possible Schmidt layouts is the main topic of the paper.

2. OPTICAL SYSTEM REQUIREMENTS

The shower of particles induced as the cosmic rays and neutrinos interact with the atmosphere presents a radial extension of about 1 km [5]. A space system observatory is supposed to operate from a height of about 300 km above the Earth's surface, and the ideal configuration would be that each detector pixel covers an atmosphere portion corresponding to an area on ground of about 1 km^2 in size, i.e. the dimension of the extended shower of particles caused by cosmic ray hit. This sets the angular resolution of the system. Therefore, if one assumes an orbit height of 300 km, the angular resolution is about 0.1°. A system having a

focal ratio $(F/_\#)$ of about 0.7 and an aperture of 2.5 m yields to a pixel of about 6 mm diameter. Under such conditions we are far from the diffraction limit, so that the geometrical optics approximation is appropriate. These basic design requirements are summarized in Tab 1.

Tab. 1. Basic system design parameters.

Field of View (FOV)	± 25°
Entrance Pupil Diameter (EPD)	2.0-2.5 m
F/#	≥ 0.7
Operating wavelengths	300-400 nm,
Angular resolution	~ 0.1°
Pixel diameter (and spot size)	~ 6 mm
Image resolution size on ground	~ 1 x 1 km^2
Operational Lifetime	3 years

A reflecting mirror with a Schmidt corrector seems to match most of the needed optical technical requirements. Nevertheless, a single mirror allows a considerable cost and mass reduction. A single mirror will be providing a large FOV and a large collecting area, in order to monitor a sufficiently large portion of Earth's surface, and to collect enough fluorescence light from orbit. A concave spherical mirror is always affected by spherical aberration; the role of a Schmidt corrector is therefore to transfer the aspheric correction from the primary to the refracting corrector at its center of curvature. The shape of the corrector causes the incoming rays to be slightly bent, so that when they are reflected by the mirror they reach focus together. The corrector adds the opposite amount of spherical aberration to the system, which causes the error to be canceled out, suppressing the spherical aberration of a spherical mirror.
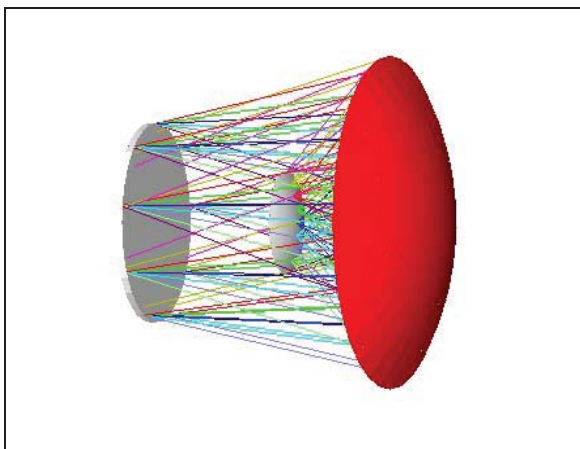

Fig. 1. The proposed layout of the Schmidt camera for high energy cosmic rays detection from space.

There are, of course, some drawbacks. The focal surface is curved on a convex surface and lies inside the instrument. Moreover, an uncorrected chromatic

aberration is introduced, depending on the wavelength (the spherochromatism), which is by far the most significant residual error in a classical Schmidt telescope with a single corrector plate. In fact, since a Schmidt corrector is a refracting element, it causes chromatic aberration, but the aberration is not severe and can be minimized by the location of the neutral zone, i.e. the zone where the corrector is the thinnest and the rays pass through it without deviation.

The central obstruction made by the focal surface is a limiting element of the design, therefore the dimension of the central focal surface detector is one of the main system performance drivers. The smaller the focal surface detector, the smaller the obstruction. At $F/_\#=1$, with a ± 25° FOV the focal plane is about the same dimension of the aperture, thus intercepting most of the rays. However, the configuration with the Schmidt camera allows lower $F/_\#$, reducing this problem, as well documented in the literature, where examples of a Schmidt camera with $F/_{0.35}$ are reported [6]. At the same time, the detector weight is reduced, which is a considerable advantage for a space based instrument. Figure 2 shows the obscuration ratio *vs*. the $F/_\#$ for a Schmidt camera with a 2-m aperture. Several curves are drawn corresponding to different limiting angles for the overall system. It is clear that a lower $F/_\#$ provides a smaller focal plane surface with a consistent reduction of the detector mass.
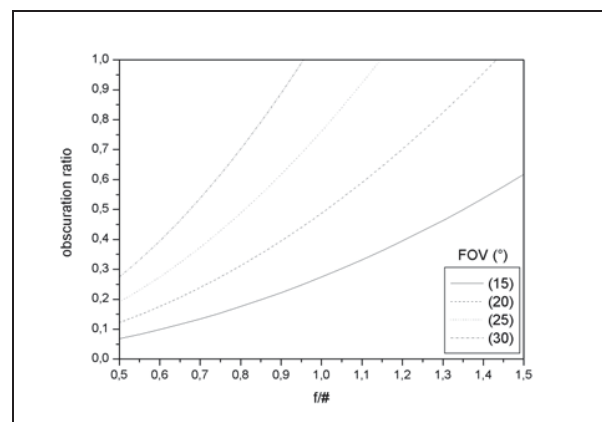

Fig. 2. Obscuration ratio of a 2m Schmidt camera with F/# at different limiting field angles.

3. OPTICAL SYSTEM DESIGN

In order to match the above mentioned basic system requirements, a first design based on a spherical primary mirror configuration has been set up. Optimization and analysis is done by ray-tracing technique aimed at maintaining the spot diagram diameter within the pixel size of 6 mm, assuring at the same time a good vignetting factor and a high amount

of energy falling into 6x6 mm^2 spot. The Root Mean Square (RMS) spot radius was calculated with reference to the centroid, defined as the central ray of the distribution of rays traced, and computed through a Gaussian quadrature algorithm.

The system was optimized monochromatically at 357 nm, the central line of fluorescence light emission supposed to be observed. A good optimization was obtained by setting zero the 2nd order aspheric term of the Schmidt corrector, giving the aspheric correction to the desired surface only through the 4th and 6th order terms.

Spot diagrams of the optical system optimized on axis are shown in Fig. 3 for incident angles from 0° to 25°. The shape and size of spot diagrams change with the wavelength and the incident angle of the incoming rays. The spot-size distribution as a function of incident angle shows that 6 mm pixel size is matched up to 17.5°, while at higher entrance angles the spots blur considerably.
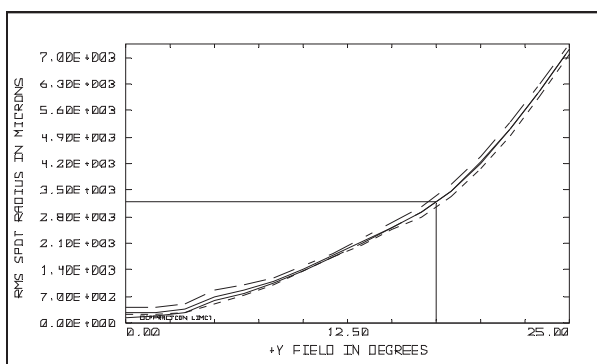

Fig. 3. RMS distribution of spot size with incident angle for optimized optical system on axis; the box shows the region where the 6 mm pixel size is matched.

Fig. 3 reveals that the system is far from the diffraction limit, which is hardly gained even for central rays in a system optimized on axis. The geometrical optics is therefore an appropriate approximation for the description of this optical system. Since a good performance on axis is not crucial, another optimization can be performed, in order to preserve the desired RMS spot radius even at larger angles. This can be done by defocusing the system for central fields, either by moving the focal plane closer to the primary mirror or by increasing the curvature radius of the focal plane. The overall result is shown in Fig. 4, where the dimensions of spot diagrams are comparable for all directions, and the RMS spot radius is homogeneous over the entire field. The plot shows some differences depending on the wavelength, resulting in a smaller spot diagram for a higher wavelength. The three curves start to match together for angles of about 18°, and follow a common path starting from this value on, overcoming slightly the 3 mm spot radius limit.
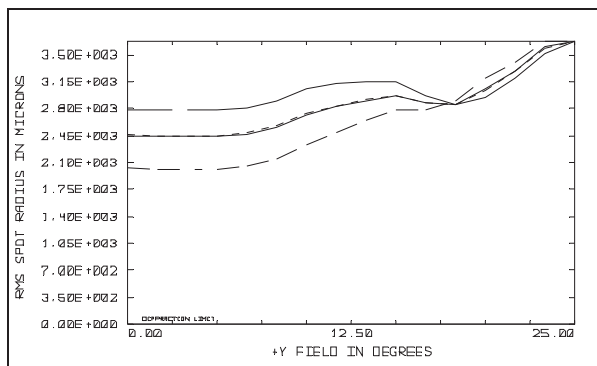

Fig. 4. RMS distribution of spot size with incident angle for optimized optical system off axis. The 3 curves shown are related to the 337, 357 and 391 nm wavelength. The polychromatic behavior (continued line) is also shown.

The performance of the system may be further improved by using an aspheric mirror as a primary. Although the manufacturing of an aspheric surface of large dimensions is not straightforward, the achievement obtained with such a mirror is notable. As in the previous case, the system was here optimized monochromatically at 357 nm. The optimization is run by maintaining free only the curvature of the primary along with its conic constant, as well as the aspheric coefficients of the corrector plate, allowing a very efficient calculation routine.
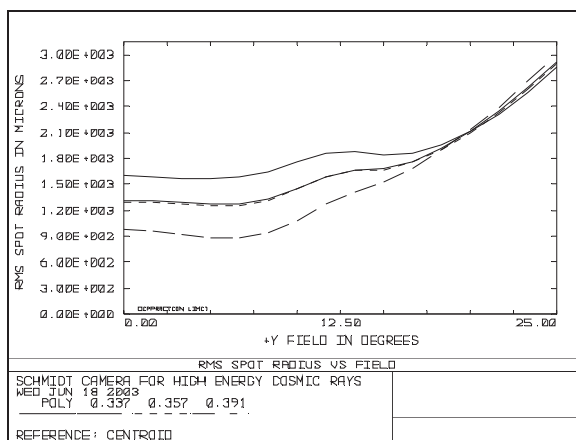

Fig. 5. Optical design with aspheric primary: RMS spot size with field angle for the 3 wavelength of interest: 337, 357, and 391 nm.

Fig. 5 illustrates that the RMS spot size is significantly reduced, compared to spherical case. The RMS spot distribution over the field shows again some differences depending on the wavelength: the higher the wavelength, the larger the blur. However, the dimension of the RMS spot radius is quite small, if compared to the previous case with the spherical primary mirror. The three curves match together from

18° on, as already observed above, remaining always under the limit of 3 mm up to 25°, while in Fig. 4 they end above this limit.

4. OPTICAL PERFORMANCE ANALYSIS

A classical way to assess the optical performance of an optical system is the evaluation of the spot diagram dimension, which is the square root of the variance of the distribution of ray intersections with the image surface. This is the best solution for systems far from diffraction limit, like this case, having more than one wave of aberration, otherwise the RMS wavefront assessment is preferred. In this case it was noticed that RMS spot size changes drastically with the field selected for the optimization. This is not surprising, as the angle of optimization sets the optical design and drives the system. Fig. 6 shows the best performance of the system at different optimization angles. This has to be intended as the theoretical achievable resolution limit of the telescope, giving immediately an idea of the minimum RMS spot radius one can get, when the system is optimized at a particular angle. At narrow entrance angles (up to 10°) no significant difference in performance is seen. When the system is optimized at higher entrance angles, the RMS spot size dimension grows linearly with the field of optimisation. At central field the spot starts significantly to increase only when the system is optimized for angles higher than 20°, affecting the performance of the system at narrow angles.
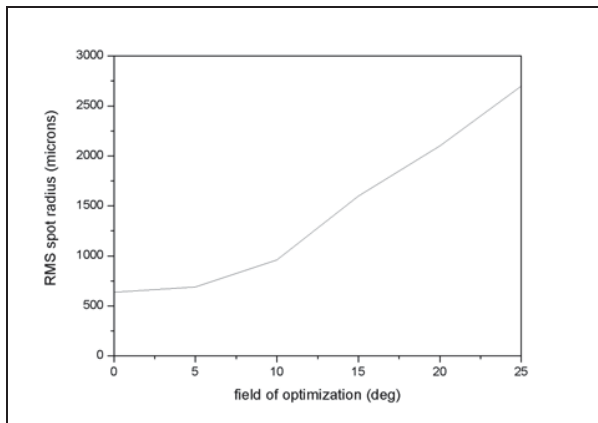

Fig. 6. RMS spot size dimension changes for central and marginal field angles with different field of optimization

The tolerances involved in the mechanical deployment system are not stringent for the present design, because of the relatively large spot dimensions. The angular tolerances for the mirror surface result to be several mrad, easily achievable with mechanical systems without any in-orbit adjustment. Requirements on the mirror alignment tolerances are then much more relaxed with respect to a classical telescope for astronomical observation or other imaging optical systems. The fact that mirrors can be supported from behind is an additional advantage in the mechanical design.

As a baseline tolerance analysis, we have evaluated the change in the RMS spot radius for each of the extreme values of the tolerance imposed to the optical elements of the design. A Monte Carlo analysis simulated the effect of all the perturbations simultaneously. The simulation has been run for each wavelength separately and the results are shown in Fig. 7, where the unperturbed RMS spot radius for the polychromatic case is compared to the minimum and maximum deviation for 337, 357, and 391 nm.
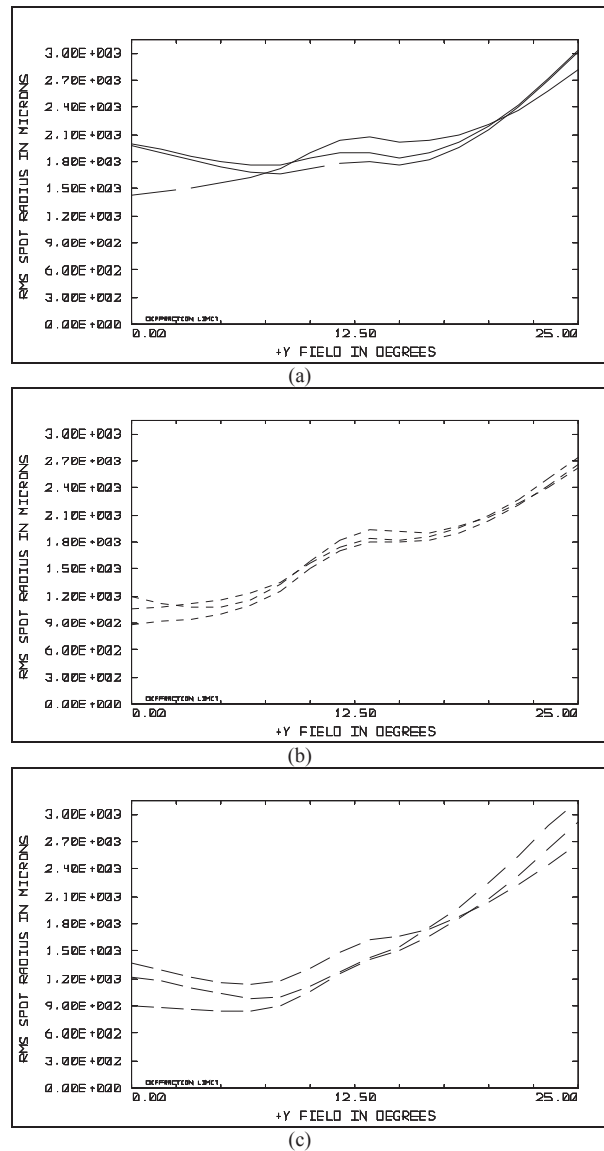

(a)

(b)

(c)

Fig. 7. RMS spot radius variation with tolerances imposed to the optical elements of the design at 337 nm (a), 357nm (b), 391 nm (c).

The RMS spot radius at 337 nm seems to be quite affected by eventual perturbations in optical parameters. At the shortest wavelength the RMS spot size is the highest among the three wavelength investigated (Fig. 7a). Moreover, the tolerance analysis indicates here a mean value of 2.25 mm over the field with a standard deviation of 0.05 mm. Fig. 7a shows also considerable variations in RMS spot radius at narrow angles rather than at higher entrance fields.

The system has the highest tolerance for the central 357 nm wavelength. In fact, the curves obtained in Fig. 7b do not differ much from those in Fig. 5. This is not surprising, as the entire optical design was optimized for this wavelength, being the one with the highest emission intensity among the three. A higher value of the RMS spot radius is also obtained at 397 nm (Fig 7c) when some tolerance is released to optical parameters. The longest wavelength showed the smallest spot among the three, while here the maximum mean value of the spot over the entire FOV is 2.20 mm, with a high standard deviation of 0.18 mm.

5. RETROFOCUS TELESCOPE

The principle of the retrofocus telescope does not differ so much from the above-described Schmidt camera, as it is a combination of mirrors and a thin aspheric refractive corrector. However, if this telescope allows a wider FOV, it must deal with the presence of obstructions which reduce the FOV at small angles. Nevertheless, this option is interesting because for the purpose of reconstructing the showers it is more advisable to have signal from the periphery of the FOV rather than from the centre.

More in detail, a primary spherical negative mirror collects the light and sends it towards the aperture stop, where the Schmidt corrector is placed. Then, light travels to the secondary positive mirror and finally is focused on the focal surface. Besides the usual optimization design issues, what makes a real challenge is the dimension of the primary mirror: indeed, depending on the scale of the design, this optical element can become as big as about twice the secondary. This concept had already been used for past projects [7], but for the purpose of detecting fluorescence the entrance pupil must have an aperture of at least 2 m, which forces the design to be quite big. Here a version suited to this topic has been preliminarily designed (Fig. 8), using two spherical mirrors and a thin aspheric corrector, with $F/_\#$ less than 1, EPD about 2.2m diameter and FOV ranging from ±17° to ±42°.
Such design forces to imagine the primary mirror as an inflatable structure: that is the reason why it has been left spherical. In the next future the design will

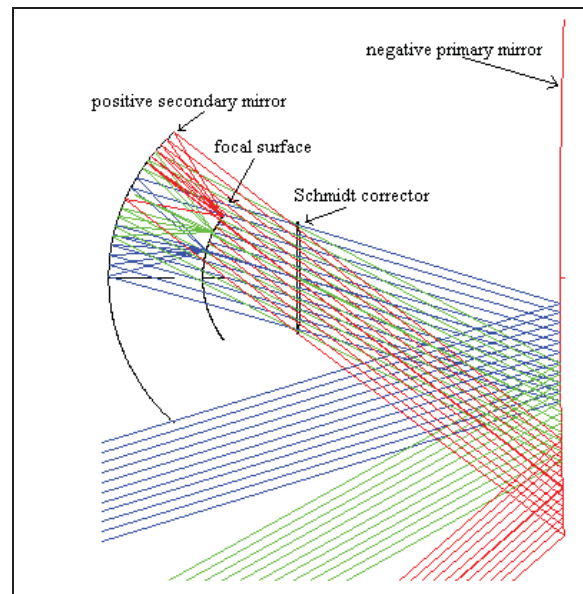improve heading towards a bigger FOV (up to 120°) while maintaining similar dimensions.

Fig. 8. Retrofocus telescope.

For the optimization of such a configuration, a trade-off is unavoidable between the amount of obscuration due to secondary mirror and focal surface and the maximum FOV, since the focal surface increases as the field.
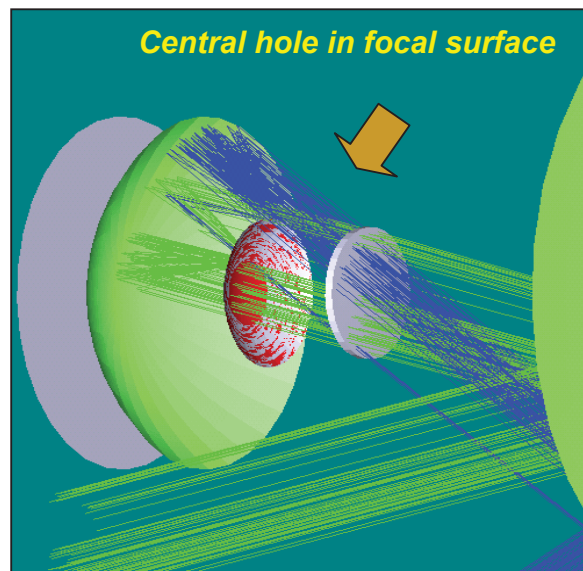

Fig. 9. Detail of focal surface obstruction.

Small angles are already obscured by the dimensions of the secondary, therefore the central zone of the focal surface is not used. As a consequence, this part can be reutilized to collect more flux from the other fields.

This is the principle depicted in Fig 9: a hole in the middle allows passing more light, thus reducing the vignetting of the spots. Fig. 10 depicts a choice of three spots from this preliminary configuration.
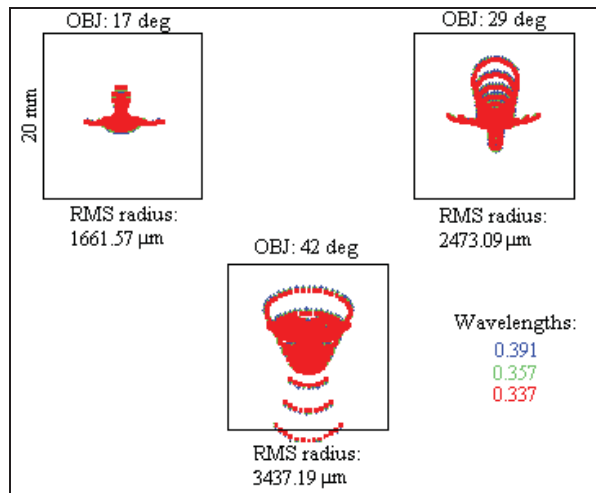

Fig 10. Spot Diagram for three fields: 17°, 29° and 42°.

6. CONSTRUCTION TECHNOLOGIES

The mirror of the Schmidt camera presented in this work is considerably large, exceeding the dimensions of the available spacecraft for space transportation, therefore a segmented mirror to be opened once in orbit has to be considered. The simplest deployment mechanism could be to divide the mirror into a fixed centre structure, about the same size of the focal plane, surrounded by a "petals" structure forming the remaining mirror. The whole could be closed around the focal plane and the corrector plate, achieving a compact cylindrical structure with a diameter close to that of the entrance pupil. The length will result about twice the focal length, or even less if a system to reduce the distance from the mirror to the focal plane is reduced. A similar structure has already been proposed for lidar application from space, and it is currently under study [8].

A possible technology for the mirror in such design could the nickel electroforming replica. The replication technique by nickel electroforming is a well known technology used to obtain thin, lightweight and good quality mirrors. Further advances in this technology may provide significant reductions in the thickness and consequently weight of the mirrors. These results have been achieved without degradation of the mirror optical quality and this technique is still far from being fully exploited. The electroforming technique is ideally suited for the production of many identical mirrors from one master, all being then assembled together to form a segmented, deployable axis-symmetrical reflector, with considerable gain in terms of costs and weight. The thermal properties of metallic mirrors will induce uniform temperature changes due to the space environment, preventing from eventual radiation-induced aberration, a typical problem one has to deal with in space, when other material like plastics is used. Metals show predictable thermal properties, enabling to predict the performance of the mirror at a wide range of temperatures with a high degree of reliability.

7. CONCLUSION

We have presented the conceptual design of a new type of telescope for HECR detection based on a wide-field Schmidt reflector. Preliminary design shows that a FOV of ± 25°, with an angular spot size resolution of 0.1° and transmission of about 70% almost independent of the field angle, can be easily achieved, being based on an easy-to-realize and well understood technology. Better performance is obtained with a design including an aspheric primary mirror. The potential of this design can open new gates in the field of HECR and astroparticle physics through high-resolution observations.

8. REFERENCES

1. Inoue, N. et al., *Shower Development of EHE Cosmic Ray*, proceedings of the International Workshop on *Space Factory on International Space Station*, Ebisuzaki T., Takahashi Y. and Hanada T. editors, Universal Academic Press, Inc., Tokyo, Japan (2000).
2. Chiba et al., *Akeno Giant Air Shower Array (AGASA) covering 1000 km² area*, Nucl. Instr. Methods, A311, 338-349, 1992.
3. Bird D. J. et al., *The Cosmic Ray Energy Spectrum Observed by the Fly's Eye,* Ap. J., 424, 491, 1993.
4. Wang S. et al., *Special configuration of a very large Schmidt telescope for extensive astronomical spectroscopic observation*, Applied Optics, 35, 25, September 1996.
5. Kakimoto F. et al., *A measurement of the air fluorescence yield*, ICRR-Report- 346-95-12, 1995
6. de Vany A. S., *Optical Design for Two Telescopes*, Applied Optics, 2, 2, February 1963.
7. Schmidtobreick L., et al., *Photographic surface photometry of the Southern Milky Way*, Astronomy and Astrophysics Supplement Series, Vol. 132, 21-27, 1998.
8. Mazzinghi P., et al., *An ultra-lightweight, large aperture, deployable telescope for advanced lidar applications, ICSO 2006*